12-2010

Femoral loading mechanics in Virginia opossums (Didelphis virginiana): torsion and mediolateral bending in mammalian parasagittal locomotion

William Gosnell
Clemson University, wgosnel@clemson.edu

FEMORAL LOADING MECHANICS IN VIRGINIA OPOSSUMS (DIDELPHIS VIRGINIANA): TORSION AND MEDIOLATERAL BENDING IN MAMMALIAN PARASAGITTAL LOCOMOTION

A Thesis
Presented to
the Graduate School of
Clemson University

In Partial Fulfillment
of the Requirements for the Degree
Master of Science
Biological Sciences

---

by
William Casey Gosnell
December 2010

Accepted by:
Dr. Richard Blob, Committee Chair
Dr. Timothy Higham,
Dr. John DesJardins

ABSTRACT

Studies of limb bone loading in terrestrial mammals have typically found anteroposterior bending to be the primary loading regime, with torsion contributing minimally. However, previous studies have focused on large, cursorial eutherian species in which the limbs are held essentially upright. Recent *in vivo* strain data from the Virginia opossum *Didelphis virginiana*, a marsupial that uses a crouched rather than upright limb posture, have indicated that its femur experiences moderate torsion during locomotion as well as strong mediolateral bending. The elevated femoral torsion and strong mediolateral bending observed in opossums (compared to other mammals) might result from external forces such as a medial inclination of the ground reaction force (GRF), internal forces deriving from a crouched limb posture, or a combination of these factors. To evaluate the mechanism underlying the loading regime of opossum femora, we filmed opossums running over a force platform, allowing us to measure the magnitude of the GRF and its three-dimensional orientation relative to the limb, facilitating estimates of limb bone stresses. This three-dimensional analysis also allows depiction of muscular forces (particularly those of hip adductors) in the appropriate anatomical plane to a greater degree than previous two-dimensional analyses. At peak GRF and stress magnitudes the GRF is oriented nearly vertically, inducing a strong abductor moment at the hip that is countered by femoral adductor muscles on the medial aspect of the bone that place this surface in compression and induce mediolateral bending, corroborating and explaining the patterns identified from strain analyses. The crouched orientation of the femur during stance in opossums also contributes to levels of femoral torsion as high as

those seen in many reptilian taxa. Femoral safety factors for bending (8.1) and torsional (18.6) loads were as high as those of reptiles and greater than those of upright, cursorial mammals, primarily because the load magnitudes experienced by opossums are much lower than those of most mammals. Thus, the evolutionary transition from crouched to upright posture in mammalian ancestors may have been accompanied by an increase in limb bone load magnitudes.

TABLE OF CONTENTS

PAGE

TITLE PAGE i

ABSTRACT ii

LIST OF TABLES v

LIST OF FIGURES vi

INTRODUCTION 1

MATERIALS AND METHODS 3

RESULTS 14

DISCUSSION 19

REFERENCES 24

LIST OF TABLES

PAGE

Table 1. Anatomical data from hindlimb muscles
of experimental animals (*D. virginiana*).....30

Table 2. Anatomical data from femora
of experimental animals (*D. virginiana*).....31

Table 3. Mean peak ground reaction force
(GRF) data for D. virginiana.....32

Table 4. Mean peak stresses for femora of D. virginiana
with GRF magnitudes and orientations at peak tensile stress.....33

Table 5. Mechanical properties and
safety factors for opossum femora.....34

LIST OF FIGURES

PAGE

Figure 1. Outline sketch of the
hindlimb skeleton of Didelphis virginiana 35

Figure 2. Representative kinematic profiles
of hindlimb joints for opossums during
a walking step over a force platform 36

Figure 3. Representative still images in
lateral (A) and posterior (B) views from
high-speed video of an opossum running over
a force platform during experimental trials 38

Figure 4. Mean ground reaction force
(GRF) dynamics for the right hindlimb of opossums 39

Figure 5. Moments exerted by the GRF
about the hindlimb joints
and the long axis for the right femur of opossums 40

Figure 6. Components of
bending stress in the femur 42

Figure 7. Loading regime
of the right femur at peak tensile stress 43

INTRODUCTION

For most tetrapod vertebrates, limb bones play a critical role in the support of the body and transmission of muscular and propulsive forces. The forces to which limb bones are exposed during terrestrial locomotion likely impose some of the highest loads that these structures experience (Biewener, 1990; Biewener, 1993). However, a growing body of data now indicates that substantial differences in loading mechanics (both loading regimes and magnitudes) are present among tetrapod lineages with different characteristic locomotor patterns. Early studies of mammals running with upright, parasagittal limb postures indicated that anteroposterior bending was generally the most important loading regime, and that the ratio of limb bone strength to load magnitude (i.e., safety factor) was generally between 2 and 4 (Rubin and Lanyon, 1982; Biewener et al., 1983; Biewener et al., 1988). In contrast, more recent data from amphibians and reptiles that use sprawling limb posture indicated prominent limb bone torsion in addition to bending, with limb bone safety factors of usually at least 5 and sometimes exceeding 10 (Blob and Biewener, 1999; Blob and Biewener, 2001; Butcher and Blob, 2008; Butcher et al., 2008). Yet, a view that such patterns have strict phylogenetic associations may not be appropriate. For example, significant torsional loading has been described for the hindlimb elements of running birds (Carrano, 1998; Main and Biewener, 2007) and rats (Keller and Spengler, 1989), species that move the limbs in essentially parasagittal planes, but which hold the femur in a more crouched position than the upright stance typical of the cursorial mammals (e.g. horses, dogs) examined in most early studies

(Rubin and Lanyon, 1982; Biewener et al., 1983). Limb posture, therefore, also appears to play a critical role in the mechanics of limb bone loading.

To help evaluate how limb bone loading patterns have diversified across clades that use different characteristic postures and locomotor kinematics, we recently analyzed *in vivo* strains from the femora of Virginia opossums (*Didelphis virginiana* Kerr) during treadmill running (Butcher et al., in review). Examination of this species helped to expand perspectives on the diversity of limb bone loading mechanics in significant ways. First, as a running marsupial, opossums belong to a lineage that is phylogenetically between the mammals and reptiles that have received previous study (Meyer and Zardoya, 2003), and could provide insight to transitions in loading patterns between these groups. Second, opossums provide additional limb bone loading data from a mammalian species that uses a more crouched limb posture (Jenkins, 1971), testing whether patterns observed in rats might hold more generally. Although strain measurements gave femoral safety factors fairly similar to those evaluated for other mammalian lineages, they also indicated significant femoral torsion in opossums in addition to bending (Butcher et al., in review). Moreover, planar strain analyses indicated a general mediolateral orientation to femoral bending (Butcher et al., in review). This result was surprising, considering that the opossums were running with essentially fore-aft oscillations of the limbs, and previous force platform data from small mammals (chipmunks and ground squirrels) had indicated anteroposterior bending of the femur in those species (Biewener, 1983).

Although *in vivo* strain data provide critical information on the distribution of loads for specific locations on bone surfaces, they are often insufficient to indicate the

mechanisms underlying the generation of the loads that are measured. To provide a complementary assessment and help evaluate the mechanisms contributing to the loading patterns of opossum femora, we evaluated the stresses developed in the femur of walking *D. virginiana* by collecting synchronized, three-dimensional kinematic and force platform data from this species. By integrating data on limb position with data on locomotor ground reaction forces, analyses of joint equilibrium can be performed to clarify both the external and muscular forces and moments acting on limb bones (Biewener and Full, 1992). Although the estimates of load magnitude that these analyses generate are indirect, significant insights into the mechanics underlying bone loading patterns can be produced (Blob and Biewener, 2001). The use of three-dimensional analyses could be particularly helpful in this regard, as most previous force-platform based analyses of mammalian limb bone loading have used two-dimensional measurements of kinematics and GRF (e.g., Alexander, 1974; Biewener, 1983; Biewener et al., 1988), with which observations of torsion and mediolateral bending would be difficult. Thus, this study will provide insight into both the specific factors contributing to the loads experienced by opossum limbs and, more generally, into the sequence of changes in limb loading mechanics through the evolutionary diversification of tetrapods.

MATERIALS AND METHODS

Animals

Force platform data were collected from four opossums, *Didelphis virginiana* (three females and one male, 1.6-3.9 kg body mass). Opossums were collected using live

traps (Havahart EasySet, 0.8 x 0.3 x 0.4 meters; Forestry Suppliers, Jackson, MS USA) in Pickens, Anderson, and Greenville Counties, South Carolina, USA. Opossums were housed at room temperature (20-23° C) in medium-sized primate enclosures (~1 m x 1 m x 0.75 m) containing a litter pan, and a pet carrier to provide cover for the animals. Opossums were exposed to 12-hour light-dark cycles and provided water and fed with commercial cat food daily. Prior to experiments, fur was shaved from the lateral aspect of the right hindlimb of each opossum, and anatomical landmarks of interest were located by palpation and marked on the skin using dots of black marker surrounded by white correction fluid. Guidelines and protocols approved by the Clemson University IACUC (AUP ARC2007-030 and 2009-059) were followed during all procedures. At the conclusion of force platform trials and complementary measurements of *in vivo* bone strain (Butcher et al., in review), opossums were anesthetized (20 mg kg^{-1} I.M. ketamine injection) and then killed by an overdose of pentobarbital sodium solution (Euthasol®, Delmarva Laboratories Inc., Midlothian, VA, USA; 200 mg kg^{-1} intracardiac injection). Experimental specimens were then frozen for later dissection and measurement of anatomical variables.

Collection of kinematic and ground reaction force data

Lateral and posterior views of running opossums were captured using a pair of synchronized high-speed digital video cameras (Phantom v.4.1, Vision Research Inc., Wayne, NJ, USA) filming at 200 Hz. Successful trials consisted of the opossums right hindlimb striking a custom-built force platform (K&N Scientific, Guilford, VT, USA)

that was inserted into a wooden trackway (for details see Butcher and Blob, 2008). The functional surface of the plate was restricted to an 11 cm × 10 cm area to increase the probability of recording isolated footfalls from a single limb. The surface of the platform was flush with the wood of the trackway, and the track and platform were coated with spray-grit and thin rubber, respectively, to reduce foot slippage.

Opossums were allowed to run at their own speed during trials and were encouraged by providing a shelter at the far end of the trackway and using a variety of stimuli, including gently squeezing the base of the tail and rubbing sandpaper or lab instruments together to create rasping noises. The trackway was kept at room temperature (20-23° C) and each opossum was allowed several minutes rest between trials, with extended rest periods when a specific stimulus no longer elicited a reaction. Trials judged suitable for initial analysis (N=16-20 per animal) showed minimal overlapping contact of the right forelimb and hindlimb on the platform.

Highlighted anatomical landmarks (hip, knee, ankle, metatarsophalangeal joint, tip of digit 4, and two points dorsal to the hip marking the anterior and posterior pelvic margins) were digitized from every frame of both lateral and posterior AVI video files using DLTdataViewer2 software (Hedrick, 2008). Three-dimensional limb kinematics were calculated from digitizing output using custom Matlab (v.7.9.0; The MathWorks Inc., Natick, MA, USA) routines that calibrated the two camera views, corrected for parallax, and allowed smoothing and normalization of traces from all trials to the same duration (101 points) by fitting quintic splines to coordinate data (Walker, 1998). Instantaneous animal speed throughout each trial also was calculated (m s^{-1}) in the

custom Matlab code by differentiating the cumulative displacement of the posterior pelvic landmark, with an average value of 1.36 ± 0.07 m/s.

The force platform resolved vertical, anteroposterior, and mediolateral components of the ground reaction force (GRF). Specifications for the platform and data acquisition system were described in a previous paper (Butcher and Blob, 2008). Force data were collected at 5000 Hz using a custom LabVIEW (v. 6.1; National Instruments, Austin, TX, USA) routine, with amplifier gains adjusted as appropriate to maximize platform sensitivity for each animal. The platform was calibrated daily in all three directions, and cross talk was negligible between force channels. The natural unloaded frequencies of each force plate component were 190 Hz, a value large enough compared to the stride frequency of opossums to limit confounding of the GRF signal.

Force and video data were synchronized using a trigger which, when activated, simultaneously produced a 1.5 V signal in the force trace and flashed an LED visible in the video. All three components of the GRF measured while the hindfoot contacted the platform were smoothed and normalized to 101 points using a quintic spline algorithm (Walker, 1998) in custom Matlab routines, matching the number of points calculated for kinematic data. For consistency with our previous force platform studies of sprawling species (Blob and Biewener, 2001; Butcher and Blob, 2008), the GRF point of application was initially calculated at the center of the portion of the foot in contact with the ground, and recalculated for each frame assuming anterior migration during stance phase (Carrier et al., 1994). The small size of opossum feet should limit any error incurred through this approach.

A custom Matlab program was used to process synchronized video and force data to calculate GRF magnitude, orientation, and moments about each hindlimb joint, producing the input for analyses of femoral stresses. Moments about the hindlimb joints induced by gravity and inertia were assumed to be negligible in our models because they are typically small relative to the moments produced by the GRF during stance (Alexander, 1974; Biewener and Full, 1992).

Model of hindlimb muscle activity and bone stress analyses

Following the approaches of our previous analyses of GRFs in sprawling taxa (Blob and Biewener, 2001; Butcher and Blob, 2008), the forces acting on the hindlimbs of opossums were resolved into an anatomical frame of reference determined by the primary planes of motion of the limb segments. However, because opossums use nearly parasagittal limb motions (Jenkins, 1971) conventions for these planes differ from those for sprawling taxa: the mediolateral (ML) plane contains both the femoral and tibial long axes, the anteroposterior (AP) plane contains the femoral long axis but is oriented perpendicular to the ML plane, and the dorsoventral (DV) plane is mutually perpendicular to the ML and AP planes. Using these conventions, extension of the ankle and knee joints occurs in the anterior direction with flexion in the posterior direction, while femoral adduction would occur in the medial direction and abduction in the lateral direction.

Femoral stress calculations similarly followed approaches established in our previous analyses of sprawling taxa (Blob and Biewener, 2001; Butcher and Blob, 2008).

Stresses were calculated at mid-shaft, where bending moments are greatest (Biewener and Taylor, 1986), and were imposed due to the action of both the GRF and muscular forces. To estimate muscle forces, limb joints were assumed to be in static rotational equilibrium; in addition, a further initial assumption was made that only muscles that would counteract the rotational moment of the GRF would be active (Alexander, 1974; Biewener, 1983a; Biewener and Full, 1992). Yet, while all muscles that cross a joint and are active during stance could contribute to moments that would counter the moment imposed on a joint by the GRF, only forces exerted by muscles spanning the mid-shaft of the femur (Fig. 1, Table 1) contribute directly to calculations of peak bending stress (Alexander, 1974; Biewener et al., 1983; Blob and Biewener, 2001; Butcher and Blob, 2008). With these assumptions, the total muscle force (F_m) required to maintain equilibrium at a joint is calculated as

$$F_m = R_{GRF} \times GRF / r_m \quad (1)$$

where R_{GRF} is the moment arm of the GRF about the joint (calculated in custom Matlab routines) and r_m is the moment arm of the muscles acting to oppose the moment of the GRF. If F_m was produced by the action of multiple muscles with different values of r_m, a weighted mean r_m was calculated for the group based on the physiological cross-sectional areas (PCSA) of each muscle, which are assumed to be proportional to the forces they exert (Alexander, 1974; Biewener and Full, 1992). Muscle moment arms were measured with digital calipers during specimen dissections with the right hindlimb held in

midstance position, and PCSAs were calculated following published protocols (Biewener and Full, 1992).

To evaluate the contributions of muscular forces to femoral stress, we constructed a model of muscle activity in the opossum hindlimb that included extensors of the ankle, flexors and extensors of the knee, and femoral adductors and retractors (Fig. 1). Consideration of all of these muscle groups was necessary to evaluate the contributions of biarticular ankle extensors to total moments at the knee joint that might elevate the forces exerted by muscles spanning the femur (Alexander, 1974; Biewener, 1983; Schoenfuss et al., in press). Because published data on hindlimb muscle activity were unavailable for opossums, our assessments of which muscles to consider followed the precedent of previous force platform-based analyses of bone loading in small mammals (Biewener, 1983) and drew from available electromyographic (EMG) data for rats and cats (Rasmussen et al., 1978; Sullivan and Armstrong, 1978; Gruner and Altman, 1980; Roy et al., 1991; Gillis and Biewener, 2001; Thota et al., 2005) to supplement anatomical assessments of function specific for opossums (Romer, 1922).

Our model included the following key features. (i) As in previous studies (Biewener, 1983; Blob and Biewener, 2001; Butcher and Blob, 2008), muscles are assumed to act in the same anatomical plane throughout stance phase. (ii) At the ankle, our model focused on ankle extensors (i.e., foot plantarflexors) because the GRF exerts a flexor moment at the ankle for most of stance (see Results). Seven muscles contribute to ankle extension, of which four only oppose the GRF moment at the ankle (flexor digitorum longus, flexor hallucis longus, soleus, and peroneus), but three are biarticular and also contribute to a

flexor moment at the knee (gastrocnemius lateralis, gastrocnemius medialis, and plantaris). (iii) Seven muscles (or muscle groups) contribute to retractor moments at the hip, but five (gluteal complex, caudofemoralis, crurococcygeus, obturator internus, and obturator externus) insert proximally and were modeled as only contributing to hip moments, while the remaining two (biceps femoris and semitendinosus) span the length of the femur (Fig. 1) and also contribute to midshaft femoral bending stresses, placing the posterior surface in compression. (iv) Knee extensors (rectus femoris and the vasti) spanning the anterior surface of the femur counter the combined knee flexor moments of the GRF and ankle extensors that span the knee. The bending moment induced by the knee extensors opposes that induced by hip retractors, placing the anterior femoral cortex in compression. (v) Five hip adductor muscles (adductor magnus, adductor longus, adductor brevis, gracilis, and semimembranosus) counter the abductor moment of the GRF at the hip (see Results), with all five spanning the midshaft. In a significant revision of previous models of bone loading in small mammals based on force platform analyses (Biewener, 1983), our three dimensional measurements of GRF moments allow the action of these muscles to be aligned with their anatomical position, rather than grouped with limb retractors. Thus, contraction of these muscles can be modeled as bending the femur to place its medial surface in compression.

Using the model outlined, muscle force calculations were made for each of the 101 time increments for each trial using the custom Matlab analysis routine. Complications with calculating muscular contributions to femoral torsion (i.e., shear stresses) due to the indeterminate nature of our modeling system led us to desist from making such estimates.

Nonetheless, the model we apply in this study accounts for known co-activation of antagonist muscle groups to the extent possible, and allows us to calculate estimates of muscles forces comparable to those from previous analyses (Biewener, 1983; Blob, 2001; Butcher and Blob, 2008).

After calculating estimates of muscle forces, bending moments along with axial and bending stresses were calculated following published methods (Biewener, 1983; Biewener and Full, 1992; Beer and Johnston, 1997) modified for three-dimensional analysis (Blob and Biewener, 2001; Butcher and Blob, 2008). Linear and angular anatomical variables (Table 2) were measured from digital photographs of the femur of each opossum. Cross-sectional anatomical variables (cross-sectional area, second moments of area, polar moment of area; Table 2) were calculated from digital photographs of mid-shaft sections cut from each bone, traced in Microsoft Powerpoint and input into custom software (Lieberman et al., 2003). Bending moments and stresses were calculated for perpendicular mediolateral and anteroposterior directions (Blob and Biewener, 2001), and accounted for bending induced by axial forces due to the moment arm of bone curvature, r_c (Biewener, 1983). Net bending stress magnitude at the mid-shaft of the femur was calculated as the vector sum of bending stresses in the anteroposterior ($\sigma_{b/AP}$) and mediolateral ($\sigma_{b/ML}$) directions (Blob and Biewener, 2001; Butcher and Blob, 2008), allowing the orientation of peak bending stress to be calculated as:

$$\alpha_{b/net} = \tan^{-1}(\sigma_{b/AP} / \sigma_{b/ML}) \quad (2)$$

where $\alpha_{b/net}$ is the angular deviation of peak stress from the mediolateral axis. This peak stress axis is perpendicular to the net neutral axis of bending. Net longitudinal stresses at the points of peak tensile and compressive bending were then calculated as the sum of axial and bending stresses. Torsional stress (τ) due to the GRF was calculated as:

$$\tau = T\,(y_t / J) \tag{3}$$

where T is the torsional moment applied to the bone by the GRF (determined from the magnitude of the net GRF and its moment arm to the long axis of the femur), y_t is the distance from the centroid of the bone to its cortex, and J is the polar moment of area (Wainwright et al., 1976). For each animal, y_t was calculated as the average of the y values from the perpendicular anteroposterior and mediolateral directions (Table 2).

Mechanical property tests and safety factor calculations

Because published data on the bending strength of opossum femora were available for the closely related species *Didelphis marsupialis* (Erickson et al., 2002), we focused our new measurements on the mechanical properties of opossum femora in torsion. Shear stresses at failure were evaluated in torsion (model 8874 biaxial testing machine with 25 kN load cell; Instron, Norwood, MA, USA) for whole bone specimens (N=7 femora) from our experimental animals, as well as additional individuals used in complimentary measurements of femoral strains (Butcher et al., in review). Procedures

closely followed those we have described previously in other studies (Butcher and Blob, 2008; Wilson et al., 2009; Butcher et al., in review). Briefly, rosette strain gauges were glued to the anterior and posterior surfaces of cleaned femora for which each end was embedded ~15 mm in dental cement. Amplified strain signals were collected while bones were twisted to failure at 3º s^{-1} (Furman and Saha, 2000), with tests performed to simulate *in vivo* medial (i.e., inward) rotation. Yield point was identified from plots of applied twisting moment *versus* maximum shear strain as the first point where measured strain magnitude deviated from the magnitude expected based on the initial, linear slope of the curve by 200 microstrain ($\mu\varepsilon$ = strain$\times 10^{-6}$; Currey, 1990). Yield stresses in torsion (shear stress) were calculated from Equation 3, using the value of T at the time of yield.

Femoral safety factors in bending were calculated as (bending strength/peak tensile stress) using the peak tensile stresses calculated from our bone stress analyses and bending strength values published for *Didelphis marsupialis* (Erickson et al., 2002). "Worst-case" safety factors in bending (Blob and Biewener, 2001) were also calculated as [(bending strength – 2 X standard deviation)/(peak tensile stress + 2 X standard deviation]. Finally, torsional yield stresses were also compared to the shear stresses on the femur induced by the GRF, but these must be regarded cautiously in the context of safety factors because these estimates of locomotor shear stress do not account for contributions of muscle forces (see above).

RESULTS

Overview of stance phase kinematics

Opossums use a plantigrade foot posture during running with a highly extended (>150°) metatarsophalangeal (MP) angle for roughly half of stance, reflecting flat placement of the hindfeet on the ground. The digits of the hindfoot point laterally from the long axis of the body. At the beginning of stance phase the femur is strongly adducted (Fig. 2, Fig. 3: mean± s.e.m.: -67±1°, where 0° is the horizontal plane) and in a slightly protracted position (mean± s.e.m.: 12±1°, where 0° is vertical). The ankle and knee joints are initially extended, but reach maximal flexion by midstance as the GRF increases. The femur undergoes a small amount of additional adduction before smoothly abducting to a peak of -56±1° shortly before the end of stance. The femur also retracts roughly 40° through the course of stance. After reaching maximal flexion the knee and ankle re-extend through most of the second half of stance. Rapid MP flexion occurs during the second half of stance as the rear of the foot is lifted from the ground. During final lifting of the foot in the last 10% of stance, the MP joint rapidly extends while the knee flexes and hip adducts in preparation for swing phase.

GRF magnitude and orientation

The GRF is oriented upwards and medially for nearly all of stance phase, and directed posteriorly for about the first third of stance before shifting anteriorly for the remainder of the step (Fig. 3, Fig. 4). Peak magnitudes of the vertical component are roughly seven times greater than those for the mediolateral and anteroposterior

components, for which peak magnitudes are similar although they occur at different times in the step (Table 3, Fig. 4). The average peak net GRF of 0.76±0.04 BW (mean ± s.e.m.) occurred at 29.7±2.9% step completion (Table 3), with a nearly vertical orientation (pooled mean at peak net GRF: AP angle, 1.0±2.2°; ML angle, -6.7±0.3°; 0°= vertical in both directions with positive values indicating anterior and lateral inclinations). The limited medial inclination of the GRF shifted even closer to a vertical (near 0°) orientation through midstance until nearly the end of the step. The combination of these GRF orientations with the position of the limb through the step produced an angle of only 10-25° between the GRF and the femur for almost all of stance (17.5±1.7° at peak GRF: Table 3, Fig. 4).

Moments of the GRF about hindlimb joints

The GRF exerts a dorsiflexor moment at the ankle for almost all of stance, until the last ~10% of the step when all but the most distal portions of the toes have been lifted from the ground (Fig. 5). The ankle moment increases early in the step and then decreases through the last three quarters of stance; nonetheless, extensors (i.e., plantarflexors) of the ankle would be expected to exert force to counter this moment for nearly all of stance, with biarticular members of this group also contributing to a flexor moment at the knee.

GRF moments about the knee and hip all shift direction during the course of stance as the limb moves forward over the foot during the step. The GRF initially exerts an extensor moment at the knee, but this shifts to a flexor moment (that would sum with

the moment imposed by biarticular ankle extensors) before midstance (Fig. 5). Thus, for the last 50-60% of stance, knee extensors would have to be active to counter this moment in order to maintain joint equilibrium. Very early in the step the GRF also exerts protractor and adductor moments at the hip; however, these both shift (to retractor and abductor moments, respectively) near 20% through the step, suggesting that while activity of limb retractors might be limited during the last three quarters of stance, activity of hip adductors would be necessary for most of the step to maintain joint equilibrium. The abductor moment appears to peak near 60% through the step, just as the mediolateral inclination of the GRF shifts to a near vertical orientation (Fig. 4).

The GRF also induces torsional moments on the femur that shift during the course of the step (Fig. 5). For the first fifth of stance (essentially matching the time during which the GRF exerts an adductor moment), these would tend to cause the right femur to rotate counterclockwise when viewed from its proximal end (i.e., inward rotation). Thereafter, the GRF, would tend to rotate the right femur clockwise when viewed from its proximal end (i.e., outward rotation), reaching a peak moment at near 60% stance.

Femoral stresses

Transverse components of the GRF impose substantial bending stresses in opossum femora in both the AP and ML directions, and the axial component of the GRF also imposes significant ML bending stress due to bone curvature (i.e., the medial offset of the femoral head to the shaft) (Fig. 6). Stresses due to these external forces are greatest early in the step (20-40%), when the net GRF is at its highest magnitude (Table

3). At their peaks, these forces tend to place the lateral surface of the femur in tension and the anterior surface in compression (Fig. 7). However, the limb muscles make the largest contribution to femoral bending stress in opossums, particularly in the ML direction. These peaks occur later in the step (near 60% stance) than those induced by external forces (Fig. 6). Contraction of knee extensor muscles in opposition to the combined knee flexor moments of the GRF and biarticular ankle extensors place the anterior surface of the femur in compression, while contraction of hip adductors places the medial surface in compression (and produces complementary tension on the lateral surface) (Fig. 7).

The opossum femur is loaded in axial compression and torsion as well as bending. Maximum tensile, compressive, and shear stresses occurred nearly simultaneously in each step, averaging between 55% and 60% stance across all trials (Table 4, Fig. 7). This is considerably later than peak net GRF (near 30% stance: Table 3), though GRF magnitudes have typically not shown major declines by this point in the step (Fig. 4), and hip abductor moments (Fig. 5) that might lead to elevated hip adductor forces and imposed stresses (Fig. 6) are at their maximum as the medial inclination of the GRF becomes nearly vertical (Fig. 3, Fig. 4). At the time of peak tensile stress, the net plane of bending (i.e., angle of the neutral axis from the anatomical ML axis) tended to place the lateral cortex in tension and the medial cortex in compression (Fig. 7). This distribution of loading reflects the significant role of the adductor muscles in our model (Fig. 1).

Peak tensile and compressive stresses for opossum femora averaged 27.3±1.2MPa and -35.5±1.7 MPa, respectively, with no clear correlation with speed across the range

used by the animals in our study. Peak compressive stresses exceed peak tensile stresses during stance (Table 4) because axial compression -4.1±0.4MPa) is superimposed on bending. Peak femoral shear stresses (3.1±0.2MPa) typically exceed axial compression (Table 4); moreover, as noted in the Materials and Methods, these values are minimum estimates that reflect only the rotational moment exerted by the GRF, and do not account for torsion produced by limb muscles.

Femoral mechanical properties and safety factor calculations

Femoral yield for opossums in bending [mean±s.e.m.: 222±12.3 MPa based on data from *D. marsupialis* (Erickson et al., 2002)] occurred at much higher stress magnitudes than femoral yield in torsion (mean±s.e.m.: 57.6±5.2MPa based on data from *D. virginiana*: Table 5). However, peak bending stress magnitudes are also likely much higher than peak shear stress magnitudes. Without accounting for torsional stresses imposed by limb muscles, the difference between bending and torsional stress is considerable (27.3±1.2MPa versus 3.1±0.2MPa, respectively: Table 4), though our calculations of torsional loading likely underestimate the total shear stress on the femur to some degree. The differences in both loads and mechanical properties of opossum femora between bending and torsion generate estimates of safety factor for these regimes of 8.1 versus 18.6 (Table 5), with the more reliable estimate for bending falling within the range of 5-10 typically reported for reptiles in previous studies. "Worst-case" estimates of safety factor are 6.6 for bending and 13.5 for torsion, again reflecting the likelihood that parasagittally running opossums place demands on their limb bones similar to the

margin of failure seen in non-mammalian species, and higher than other mammals that use more upright limb posture.

DISCUSSION

Loading regimes in opossum femora: the significance of torsion and mediolateral bending

The opossum femur is loaded in a combination of axial compression, bending, and torsion. While axial compression and bending were expected based on previous studies of limb bone loading in mammals (Biewener 1983; Biewener et al., 1983; Biewener et al., 1988), the significance of torsion was more surprising. Correlated with the use of upright limb posture and parasagittal kinematics, particularly among larger species (e.g. dogs, horses), most previous studies of mammalian limb bone loading had found (or assumed) negligible torsion in mammalian hind limb bones during locomotion (e.g., Alexander, 1974; Rubin and Lanyon, 1982; Biewener 1983; Biewener et al., 1983; Biewener et al., 1988). However, the average magnitude of shear stress induced by the GRF in opossum femora (3.1±0.2MPa) is similar in magnitude to that measured from many reptilian and amphibian species [1.0-5.8 across salamanders, lizards, and crocodilians (Blob and Biewener, 2001; Wright et al., 2007)]. These results corroborate findings of significant shear strains in opossum femora (Butcher et al., in review), and are in line with findings of moderate to substantial torsional loading in the femora of rats (Keller and Spengler, 1989) and terrestrial birds (Carrano, 1998; Main and Biewener, 2007). These species, like opossums, also use near-parasagittal limb kinematics and hold

the femur in a crouched position for much of stance. Given that GRF orientation during periods of peak loading is essentially similar across a wide range of species from amphibians to mammals, and spanning sprawling to upright posture (Jayes and Alexander, 1980; Biewener, 1983; Blob and Biewener, 2001; Butcher and Blob, 2008), these data indicate that differences in loading regimes across taxa are primarily influenced by their different limb postures. They also suggest that torsional loading may be a persistent, ancestral feature of tetrapod limb mechanics until fully upright posture is adopted.

Although bending was expected for opossum femora, the direction of bending that was identified was unexpected based on their parasagittal limb kinematics. Previous studies of mammalian limb bone loading (e.g., Biewener, 1983; Biewener et al., 1983) had identified primarily anteroposterior bending, although some of these studies were based on only two dimensional force data with a limited capacity to measure bending out of this plane. In an additional corroboration of results from *in vivo* strain measurements, our force platform data also indicated a fairly close alignment of the neutral axis of bending with the anatomical anteroposterior axis, such that the medial surface of the femur was placed in tension and the lateral surface in compression (Fig. 7). This orientation indicates a surprisingly strong divergence of the direction of femoral bending from the direction of travel; however, our model of muscular forces acting on the femur provides insight into how this pattern arises.

Our use of a three-dimensional analysis allows the action of medially situated adductor muscles to be modeled in their most appropriate anatomical plane, rather

grouping these muscles with posteriorly situated limb retractors as in previous studies (Biewener, 1983). Because the GRF exerts an abductor moment for most of the step (Fig. 5), these adductors must be active for most of stance, contracting to place the medial surface of the femur in compression. This stress increases as the GRF becomes more vertical (Fig. 3, Fig. 4) and its hip abductor moment arm increases (Fig. 5) toward 60% of stance, even as GRF magnitude has begun to decrease from its peak near 30% stance; moreover, it is not substantially countered by the action of any hip abductor muscle spanning the length of the femur that could bend the bone in the opposite direction and reduce overall stress. The medial inflection of the femoral head from the shaft also increases the potential for axial forces in impose mediolateral bending (Fig. 6). In contrast, for bending in the anteroposterior direction, activity of hip retractors along the posterior surface of the femur appears to decrease later in the step as the GRF exerts a retractor moment itself (Fig. 5). Knee extensors on the anterior surface are active later in the step against the flexor moment of the knee (Fig. 5), but these impose stress in the opposite direction from the GRF for much of the time they active (Fig. 6), so that net anteroposterior stress is minimized. This combination of strong adductor muscle activity and minimization of bending imposed by anteriorly and posteriorly situated muscles generates the predominantly mediolateral pattern of bending (Fig. 7) despite the main anteroposterior oscillation of the limbs during running.

Safety factors in opossum femora: mechanical basis and evolutionary implications

Safety factors of the opossum femora were determined to be 8.1 in bending and potentially as high as 18.6 in torsion, though (as noted previously) this latter value does not account for torsional stresses induced by limb muscles. This value for bending is relatively similar to strain based estimates of femoral safety factors for opossums, which range between 5 and 8 (Butcher et al., in review). Though there are differences in safety factor estimates between the two experimental approaches, the presence of such differences has been noted in other comparisons of these techniques (Biewener, et al., 1983; Butcher et al., 2008).

Like the corresponding strain data, the opossum safety factors obtained through this stress analysis were moderately higher than the safety factors of other mammals and at least as high as the safety factors calculated for reptiles and amphibians in recent studies. The mechanical properties of opossum limb bones are not especially distinctive compared to those of other taxa (Currey, 1987; Erickson et al., 2002; Wilson et al., 2009). Instead, opossum safety factors are higher than those of most mammals because the magnitudes of loads they experience are lower (by a factor of two or more for some species: Table 4). An interesting question that remains is that nature of the evolutionary association between limb posture and limb bone loading magnitudes. Did upright posture help to keep increasing limb bone loads in check, or might elevated loads actually have accompanied the evolution of more upright posture? Historical data to evaluate these alternatives would be challenging to gather. However, the recognition that, within animals that use a range of limb postures, loads often increase with the use of more

upright stance (Blob and Biewener, 1999; Blob and Biewener, 2001; Reilly and Blob, 2003) suggests that the evolution of upright posture in mammals may have carried accommodation of higher limb bone loading as a consequence.

REFERENCES

Alexander, R. M. (1974). The mechanics of a dog jumping, *Canis familiaris*. *J. Zool. Lond.* **173**, 549-573.

Biewener, A. A. (1983a). Locomotory stresses in the limb bones of two small mammals: the ground squirrel and chipmunk. *J. Exp. Biol.* **103,** 131-154.

Biewener, A. A. (1983b). Allometry of quadrupedal locomotion: the scaling of duty factor, bone curvature and limb orientation to body size. *J. Exp. Biol.* **105,** 147-171.

Biewener, A. A., Thomason, J., Goodship, A. and Lanyon, L. E. (1983). Bone stress in the horse forelimb during locomotion at different gaits: a comparison of two experimental methods. *J. Biomech.* **16**, 565-576.

Biewener, A. A., Thomason, J. and Lanyon, L. E. (1988). Mechanics of locomotion and jumping in the horse (*Equus*): *in vivo* stress in the tibia and metatarsus. *J. Zool. (Lond.)* **214**, 547-565.

Biewener, A. A. (1990). Biomechanics of mammalian terrestrial locomotion. *Science* **250,** 1097-1103.

Biewener, A. A. and Full, R. J. (1992). Force platform and kinematic analysis. In *Biomechanics -- Structures and Systems: A Practical Approach* (ed. A. A. Biewener), pp. 45-73. New York: Oxford University Press.

Biewener, A. A. (1993). Safety factors in bone strength. *Calcif. Tissue Int. (Suppl. 1).* **53,** S68-S74.

Biewener, A. A. and Taylor, C. R. (1986). Bone strain: a determinant of gait and speed? *J. Exp. Biol.* **123,** 383-400.

Blob, R. W. (2001). Evolution of hindlimb posture in non-mammalian therapsids: biomechanical tests of paleontological hypotheses. *Paleobiology* **27,** 14-38.

Blob, R. W. and Biewener, A. A. (1999). In vivo locomotor strain in the hindlimb bones of *Alligator mississippiensis* and *Iguana iguana*: implications for the evolution of limb bone safety factor and non-sprawling limb posture. *J. Exp. Biol.* **202,** 1023-1046.

Blob, R. W. and Biewener, A. A. (2001). Mechanics of limb bone loading during terrestrial locomotion in the green iguana (*Iguana iguana*) and American alligator (*Alligator mississippiensis*). *J. Exp. Biol.* **204,** 1099-1122.

Butcher, M. T. and Blob, R. W. (2008). Mechanics of limb bone loading during terrestrial locomotion in river cooter turtles (*Pseudemys concinna*). *J. Exp. Biol.* **211,** 1187-1202.

Butcher, M. T., Espinoza, N. R., Cirilo, S. R. and Blob, R. W. (2008). *In vivo* strains in the femur of river cooter turtles (*Pseudemys concinna*) during terrestrial locomotion: tests of force-platform models of loading mechanics. *J. Exp. Biol*. **211,** 2397-2407.

Butcher, M. T. Bartholemew J.W., Nathan B.H., Gosnell W.C., Parish H.A., and Blob R.W. In vivo strains in the femur of the opossum (*Didelphis virginiana*) during terrestrial locomotion: testing hypotheses of evolutionary shifts in mammalian bone loading and design. *J. Exp. Biol.* (in review).

Carrano, M. T. (1998). Locomotion of non-avian dinosaurs: integrating data from hindlimb kinematics, *in vivo* strains and bone morphology. *Paleobiol*. **24,** 450-469.

Carrier, D. R., Heglund, N. C. and Earls, K. D. (1994). Variable gearing during

locomotion in the human musculoskeletal system. *Science* **265**, 651-653.

Currey, J. D. (1987). The evolution of the mechanical-properties of amniote bone. *J. Biomech*. **20**, 1035-1044.

Currey, J. D. (1990). Physical characteristics affecting the tensile failure properties of compact bone. *J. Biomech*. **23,** 837-844.

Erickson, G. M., Catanese, J. III. and Keaveny, T. M. (2002). Evolution of the biomechanical material properties of the femur. *Anat. Rec.* **268,** 115-124.

Furman, B. R. and Saha, S. (2000). Torsional testing of bone. In *Mechanical Testing of Bone and the Bone-Implant Interface* (ed. Y. H. An. and R. A. Draughn) pp. 219-239. Boca Raton: CRC press.

Gillis G.B., Biewener A.A. (2001). Hindlimb muscle function in relation to speed and gait: In vivo patterns of strain and activation in a hip and knee extensor of the rat (Rattus norvegicus). *J. Exp. Biol*. **204**, 2717-2731.

Gruner J.A., Altman J. (1980). Swimming in the rat – analysis of locomotor performance in comparison to stepping. *Ex. Brain Res*. **40,** 374-382.

Hedrick, T. L. (2008). Software techniques for two- and three-dimensional kinematic measurements of biological and biomimetic systems. *Bioinspir Biomim*. 3, 034001.

Jayes, A. S. and Alexander, R. McN. (1980). The gaits of chelonians: walking techniques for very slow speeds. *J. Zool., Lond.* **191,** 353-378.

Jenkins, F. A., Jr (1971). Limb posture and locomotion in the Virginia opossum (*Didelphis marsupialis*) and in other cursorial mammals. *J. Zool. Lond.* **165,** 303-315.

Keller, T. S. and Spengler, D. M. (1989). Regulation of bone stress and strain in the immature and mature rat femur. *J. Biomech.* **22,** 1115-1127.

Kemp, T. S. (1982). *Mammal-like reptiles and the origin of mammals*. London: Academic Press.

Lieberman, D. E., Pearson, O. M., Polk, J. D., Demes, B. and Crompton, A. W. (2003). Optimization of bone growth and remodeling in response to loading in tapered mammalian limbs. *J. Exp. Biol*. **206,** 3125-3138.

Main, R. P. and Biewener, A. A. (2007). Skeletal strain patterns and growth in the emu hindlimb during ontogeny. *J. Exp. Biol.* **210,** 2676-2690.

Meyer, A. and Zardoya, R. (2003). Recent advances in the (molecular) phylogeny of vertebrates. *Annu. Rev. Ecol. Evol. Syst.* **34,** 311-338.

Rasmussen S., Chan A.K., Goslow G.E. (1978). Cat Step Cycle – electromyographic patterns for hindlimb muscles during posture and unrestrained locomotion. *J. Morph.* **155,** 253-269.

Reilly, S. M., Blob, R. W. (2003). Motor control of locomotor hindlimb posture in the American alligator (*Alligator mississipiensis*). *J. Exp. Biol.* **203,** 4327-4340.

Romer, A. S. (1922). The locomotor apparatus of certain primitive and mammal-like reptiles. *Bull. Am. Mus. Nat. Hist*. **46,** 517-606.

Roy R.R., Hutchison D.L., Pierotti D.J., et al. (1991). EMG patterns of rat ankle extensors and tensors during treadmill locomotion and swimming. *J. Appl. Physiol*. **70,** 2522-2529.

Rubin, C. T. and Lanyon, L. E. (1982). Limb mechanics as a function of speed and gait: a study of functional strains in the radius and tibia of horse and dog. *J. Exp. Biol.* **101,** 187-211.

Sullivan T.E., Armstrong R.B. (1978). Rat locomotory muscle-fiber activity during trotting and galloping. *J. Appl. Physiol*. **44,** 358-363.

Thota A.K., Watson S.C., Knapp E., et al. (2005). Neurochemical control of locomotion in the rat. *J. Neurotraum*. **22,** 442-465.

Wainwright, S. A., Biggs, W. D., Currey, J. D. and Gosline, J. M. (1976). *Mechanical Design in Organisms*. Princeton: Princeton University Press.

Walker, J. A. (1998). Estimating velocities and accelerations of animal locomotion: a simulation experiment comparing numerical differentiation algorithms. *J. Exp. Biol.* **201**, 981-995.

Wilson, M. P., Espinoza, N. R., Shah, S. R. and Blob, R. W. (2009). Mechanical properties of the hindlimb bones of bullfrogs and cane toads in bending and torsion. *Anat. Rec.* **292**, 935-944.

Wright K.M., Butcher M.T., and Blob, R. W. (2007). Limb bone loading in salamanders during terrestrial locomotion. *J. Morph.* **268**, 1151-1151.

Tables and Figures

Table 1. Anatomical data from hindlimb muscles of experimental animals (*D. virginiana*)

	op04			op05			op06			op07		
Muscles	A	θ	r_m	A	θ	r_m	A	θ	r_m	A	θ	r_m
Ankle extension												
Flexor digitorum longus	9.7	0	3.1	22.7	0	6.5	29.0	0	7.7	12.4	0	3.2
Flexor hallucis longus	6.4	0	3.1	19.0	0	4.3	83.2	0	7.3	24.3	0	2.6
Soleus	48.8	0	5.5	73.2	0	6.0	192.6	0	8.1	101.9	0	3.2
Peroneus	40.4	0	2.4	56.2	0	2.1	217.7	0	2.5	115.2	0	1.7
Gastrocnemius lateralis	43.2	0	6.9	110.7	0	6.6	37.1	0	7.7	130.8	0	7.9
			4.6^k			6.2^k			13.5^k			6.1^k
Gastrocnemius medialis	19.4	0	8.2	47.5	0	11.0	132.2	0	11.6	37.4	0	8.1
			4.9^k			9.6^k			14.6^k			6.8^k
Plantaris	10.3	0	6.9	20.9	0	5.4	97.1	0	10.2	30.8	0	7.9
			4.0^k			7.8^k			18.9^k			6.1^k
Knee extension												
Rectus femoris	68.6	5	3.8	105.9	5	9.0	279.0	5	12.2	217.9	5	4.8
Vastus medialis	38.4	0	4.6	75.2	0	9.3	140.0	0	10.2	147.5	0	4.5
Vastus intermedius	41.9	0	3.2	40.8	0	4.5	170.3	0	10.2	140.4	0	5.9
Vastus lateralis	36.4	0	4.6	108.1	0	5.3	245.8	0	9.1	52.9	0	6.0
Hip retraction												
Gluteal complex	139.1	0	2.9	134.8	0	3.8	248.7	0	7.7	275.3	0	5.1
Caudofemoralis	19.8	0	8.7	38.7	0	14.1	44.1	0	18.9	33.7	0	12.2
Crurococcygeus	6.4	22	20.4	18.4	21	23.9	21.3	24	39.1	14.1	10	24.5
			27.1^k			30.9^k			37.6^k			24.9^k
Obturator internus	15.6	0	7.7	18.8	0	5.6	22.9	0	6.0	25.4	0	11.5
Obturator externus	41.5	0	3.7	83.8	0	7.0	98.2	0	9.3	73.1	0	2.9
Bicpes femoris	43.1	15	15.7	88.2	18	21.4	90.6	15	16.1	96.4	8	6.2
			15.2^k			16.0^k			15.2^k			18.8k
Semitendinosus	21.3	22	15.9	38.8	20	28.4	51.8	18	18.8	38.4	16	9.5
			26.8^k			18.7^k			18.3^k			17.4^k
Hip adduction												
Adductor magnus	49.7	5	11.4	97.0	20	29.7	131.6	20	11.1	37.3	15	15.3
Adductor longus	36.3	10	15.7	189.6	15	21.4	84.9	20	16.1	104.8	5	6.2
Adductor brevis	20.2	20	13.4	73.5	10	10.0	35.2	17	16.7	127.8	20	14.4
Gracilis	33.2	20	20.4	21.6	17	23.9	81.8	18	39.1	75.1	15	24.5
			17.7^k			16.8^k			29.6^k			24.5^k
Semimembranosus	46.4	20	23.4	41.5	20	26.0	108.6	19	26.6	55.2	15	15.3
			14.9^k			15.9^k			12.0^k			11.3^k

A, physiological cross-sectional area of muscle (mm^2); θ, angle between the muscle and the long axis of the femur (degrees); r_m, moment arm of the muscle (mm) about the joint indicated by the section heading or with a k for knee flexion.

Table 2. Anatomical data from femora of experimental animals (*D. virginiana*)

Measurement	op04	op05	op06	op07
Length (mm)	65.87	79.68	83.84	84.95
A (mm^2)	11.01	20.68	35.20	24.73
$r_{c(ML)}$ (mm)	-5.97	-5.57	-8.10	-6.31
$r_{c(AP)}$ (mm)	-1.30	0.45	0.67	0.57
$y_{(ML)}$ (mm)	2.23	3.80	3.74	3.18
$y_{(AP)}$ (mm)	2.04	4.16	3.65	3.27
I_{ML} (mm^4)	17.70	52.60	157.00	79.70
I_{AP} (mm^4)	20.40	62.50	164.00	86.20
J (mm^4)	38.10	115.10	321.00	165.90

In subscript notations, AP denotes the anatomical anteroposterior direction for the femur; ML denotes the anatomical mediolateral direction for the femur. *A* denotes the cross-sectional area of bone; r_c, moment arm due to bone curvature; *y*, distance from neutral axis to cortex; *I*, second moment of area; *J*, polar moment of area. Curvature sign conventions for ML: positive, concave lateral; negative, concave medial. Curvature sign conventions for AP: positive, concave posterior; negative, concave anterior.

Table 3. Mean peak ground reaction force (GRF) data for *D. virginiana*

Animal	GRF			Peak net GRF time (%)	Net GRF (BW)	GRF femur angle (deg.)	GRF AP angle (deg.)	GRF ML angle (deg.)	Running speed (m/s)
	Vertical (BW)	Horizontal (BW)	ML (BW)						
op04 (*N*=20)	0.56±0.02	-0.07±0.03	-0.08±0.01	33.0±1.1	0.58±0.01	16.87±1.3	-7.93±2.9	-8.0±1.2	1.35±0.04
op05 (*N*=13)	1.03±0.05	0.06±0.03	-0.14±0.01	30.2±1.4	1.05±0.05	14.73±1.0	2.77±1.5	-8.3±0.9	1.80±0.12
op06 (*N*=15)	0.74±0.04	0.11±0.02	-0.07±0.01	32.4±3.4	0.76±0.05	14.63±1.9	8.06±1.3	-6.2±1.3	1.28±0.09
op07 (*N*=8)	0.62±0.04	0.01±0.04	-0.05±0.02	23.3±5.7	0.63±0.05	23.68±2.8	0.93±3.2	-4.1±1.8	0.77±0.12
Mean ± s.e.m.	0.74±0.04	0.03±0.03	-0.09±0.01	29.7±2.9	0.76±0.04	17.48±1.7	0.95±2.2	-6.7±0.3	1.36±0.07

GRF femur, angle of ground reaction force to the femur; GRF AP, anteroposterior inclination angle of GRF; GRF ML, mediolateral inclination angle of GRF.

Vertical=0° for GRF AP and ML angles of inclination; for GRF AP, negative angles are posteriorly directed and positive angles are anteriorly directed; for GRF ML, negative angles are medially directed.

BW, body weight.

Values are means ± s.e.m. (*N*=number of steps analyzed).

Table 4. Mean peak stresses for femora of *D. virginiana* with GRF magnitudes and orientations at peak tensile stress

		Peak stress										
Individual	*N*	Tensile (MPa)	Comp. (MPa)	Axial (MPa)	Shear (MPa)	Peak tens. time (%)	Peak comp. time (%)	Peak shear time (%)	Neutral axis angle from ML (deg.)	Net GRF (BW)	GRF AP angle (deg.)	GRF ML angle (deg.)
op04	20	21.9±1.4	-28.4±1.9	-3.2±0.4	3.3±0.4	56.3±1.2	55.5±1.2	53.4±3.8	114.9±2.1	0.47±0.01	7.89±2.8	2.25±1.4
op05	13	34.4±2.4	-44.7±2.8	-5.1±0.4	4.5±0.3	60.7±1.5	60.1±1.5	59.6±1.9	116.1±1.0	0.66±0.03	10.0±2.0	-6.33±0.7
op06	15	23.4±2.7	-30.8±3.4	-3.7±0.4	2.0±0.3	63.9±3.4	64.4±3.3	63.5±2.0	107.1±1.7	0.49±0.03	10.0±1.0	-1.38±1.2
op07	8	36.5±2.1	-47.0±3.0	-5.3±0.5	2.7±0.2	55.0±2.8	55.8±2.9	48.6±7.5	112.9±0.9	0.48±0.03	4.38±1.2	-1.02±1.1
Mean ± s.e.m.	56	27.3±1.2	-35.5±1.7	-4.1±0.4	3.1±0.2	59.0±2.2	59.1±2.2	56.3±3.8	112.7±1.4	0.52±0.03	8.07±1.7	-1.62±1.1

Shear stresses are reported for counterclockwise rotations of the right femur as viewed from the proximal end.
Axial stresses are reported at the time of peak tensile stress.
Peak tension (tens.) and compression (comp.) time are shown as a percentage of stance.
Deviations of the neutral axis from the anatomical mediolateral (ML) axis of each bone are clockwise in direction (i.e. positive angle from horizontal at 0º).
AP, anteroposterior.
Vertical=0° for GRF AP and ML angles of inclination; for GRF AP, negative angles are posteriorly directed and positive angles are anteriorly directed; for GRF ML, negative angles are medially directed and positive angles are laterally directed.
Peak stresses were determined from force platform loading data; *N*=number of steps analyzed.
Values are means ± s.e.m.

Table 5. Mechanical properties and safety factors for opossum femora

Bending			Torsion		
Yield stress (MPa)	Peak stress (MPa)	Safety factor	Yield stress (MPa)	Peak stress (MPa)	Safety factor
222±12.3*	27.3±1.2	8.1	57.6±5.2	3.1±0.2	18.6

Values are means ± s.e.m.
*Value for *Didelphis marsupialis* (Erickson et al., 2002)

Figure 1. Outline sketch of the hindlimb skeleton of *Didelphis virginiana*

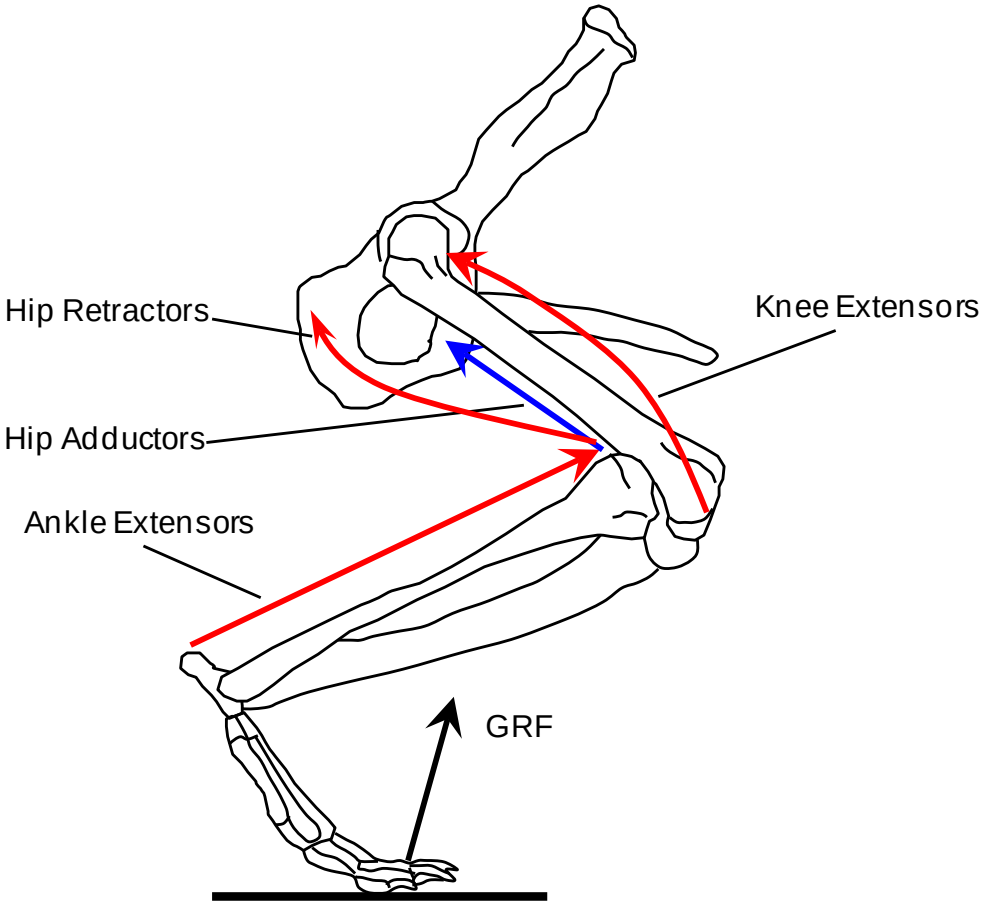

Outline sketch (right lateral view) of the hindlimb skeleton of Didelphis virginiana illustrating the lines of action of the major muscle groups contributing to stresses in the femur during the stance phase of terrestrial locomotion for the anteroposterior (red arrows) and mediolateral (blue arrow) directions. These forces are elicited in response to the GRF (black arrow). Sketch modified from Kemp (1982)

Figure 2. Representative kinematic profiles of hindlimb joints for opossums during a walking step over a force platform

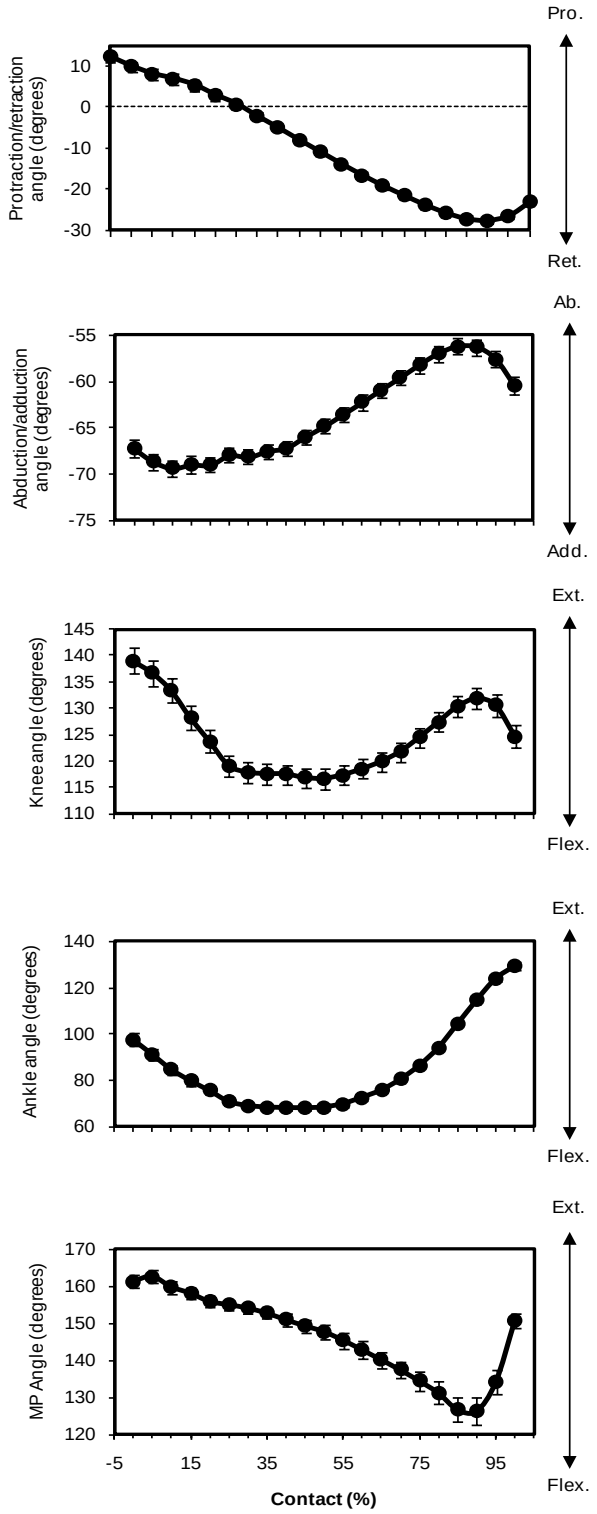

Figure 2, continued

Top to bottom: femoral (hip) protraction (Pro.)/retraction (Ret.) angle, femoral (hip) abduction (Ab.)/adduction (Add.) angle, knee, ankle, and metatarsophalangeal (MP) angles (Ext., extension; Flex., flexion). Kinematic profiles represent mean (±s.e.m.) angles averaged across all four opossums (N=8-20 trials per individual, 56 total steps per data point). Note that axis scales differ for these plots to provide increased resolution for smaller angles.

Figure 3. Representative still images in lateral (A) and posterior (B) views from high-speed video of an opossum running over a force platform during experimental trials

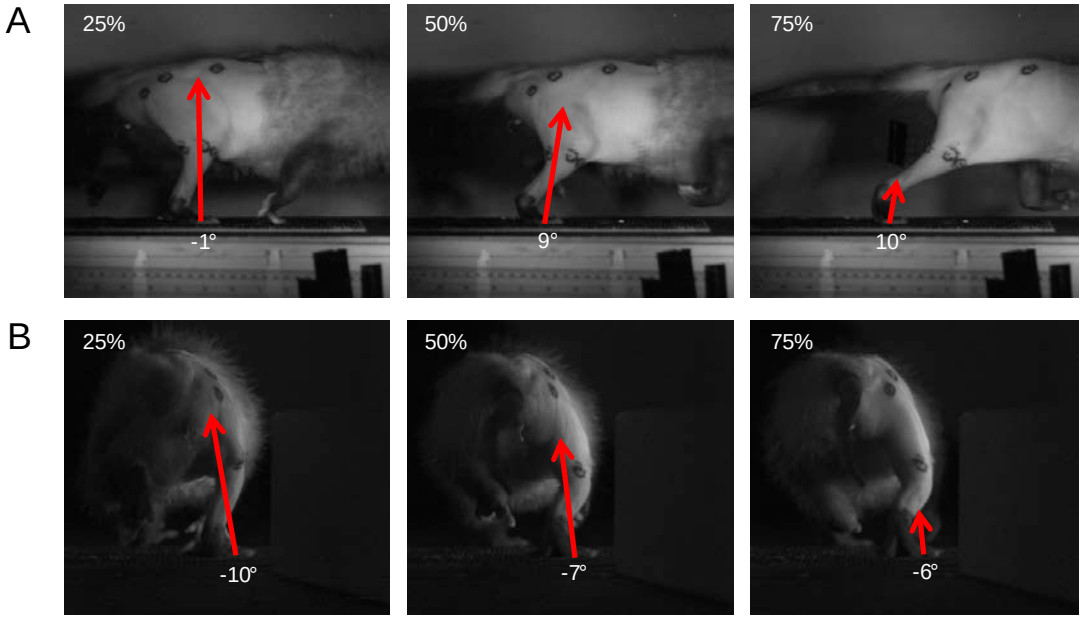

Three points in time through the course of stance are indicated (percentages labeled on each panel), and the relative magnitude and orientation of the GRF is illustrated by red arrows in each frame.

Figure 4. Mean ground reaction force (GRF) dynamics for the right hindlimb of opossums

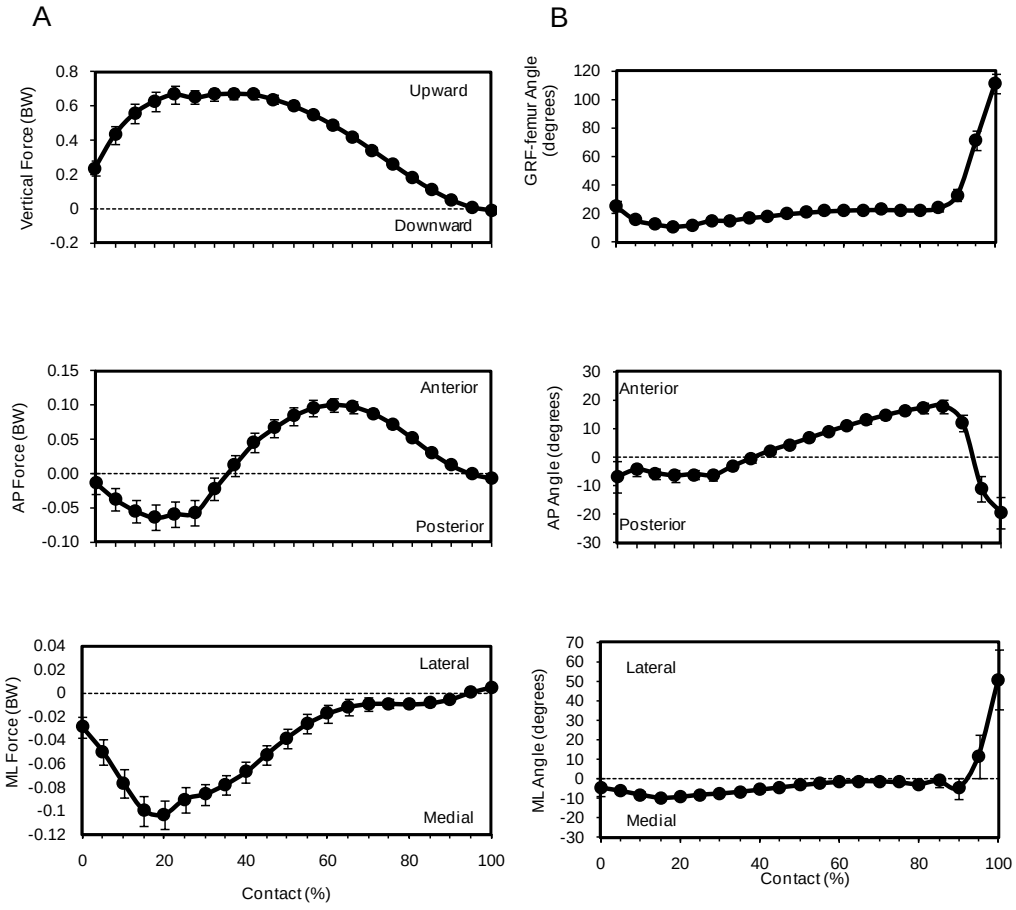

All plots show means (±s.e.m.) averaged across all four opossums (N=8-20 trials per individual, 56 total steps per data point). (A) Vertical, anteroposterior (AP) and mediolateral (ML) GRF components in body weight (BW), with positive values indicating upward, anterior and lateral forces, respectively (top to bottom). Axis scales differ for these plots to provide increased resolution for the small AP and ML forces. All trials were normalized to the same duration, allowing values to be graphed against the percentage of time through the stance. (B) Angle of the GRF (top to bottom) relative to the long axis of the femur and in the AP and ML directions. AP angles were determined relative to vertical at 0º (90º indicates GRF horizontal, pointing forward; <0º indicates posteriorly directed GRF). ML angles were determined relative to vertical at 0º (negative values indicate medially directed GRF). Femoral angles were determined relative to 0º at the femoral long axis.

Figure 5. Moments exerted by the GRF about the hindlimb joints and the long axis for the right femur of opossums

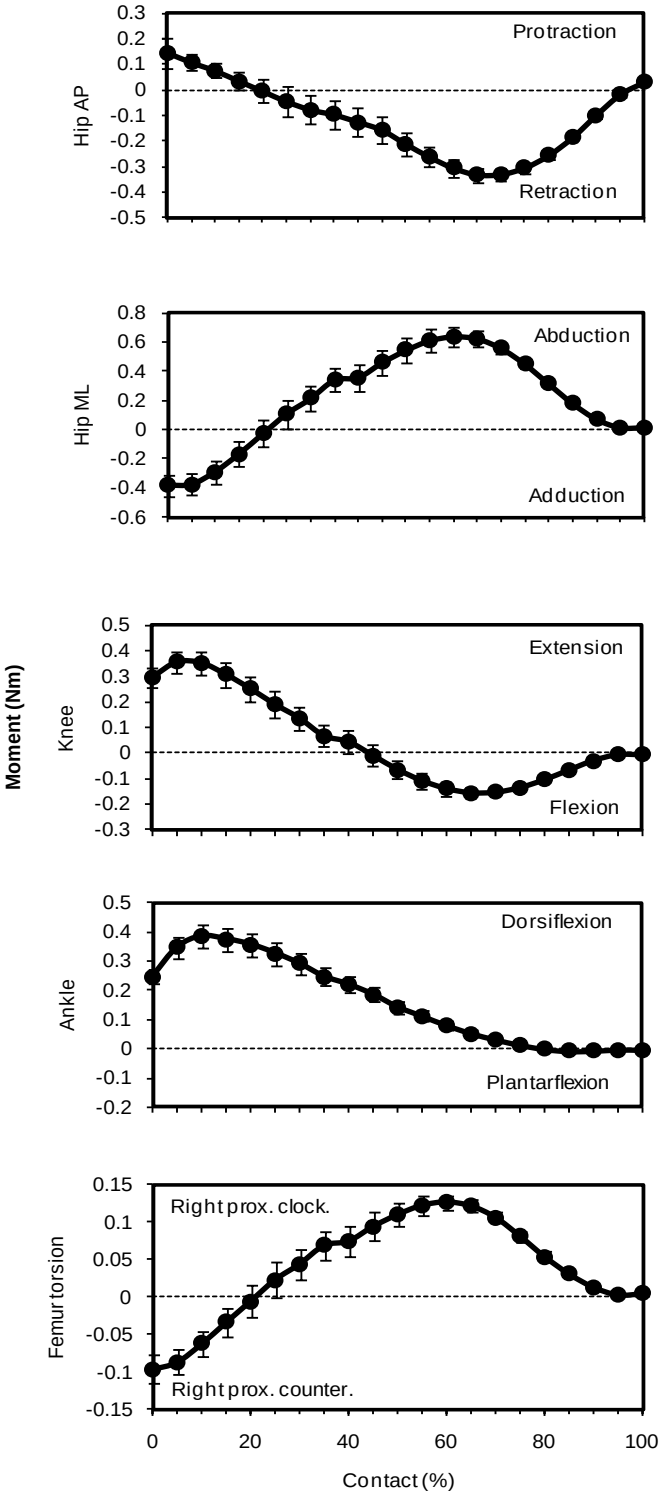

Figure 5, continued

All plots show means (±s.e.m.) averaged across all four opossums (N=8-20 trials per individual, 56 total steps per data point). Note that axis scales differ for these plots to provide greater resolution for smaller moments. Directions of moments are labeled to the right of the figure plots. Hip AP, the GRF moment about the hip in the anatomical anterior and posterior directions; Hip DV, the GRF moment about the hip in the anatomical dorsal and ventral directions; Knee and Ankle, the GRF moments about the knee and ankle joints in the medial and lateral directions; Right prox. clock., torsional GRF moment, clockwise when viewing the right femur from the proximal end; right prox. counter., torsional GRF moment, counterclockwise when viewing the right femur from its proximal end.

Figure 6. Components of bending stress in the femur

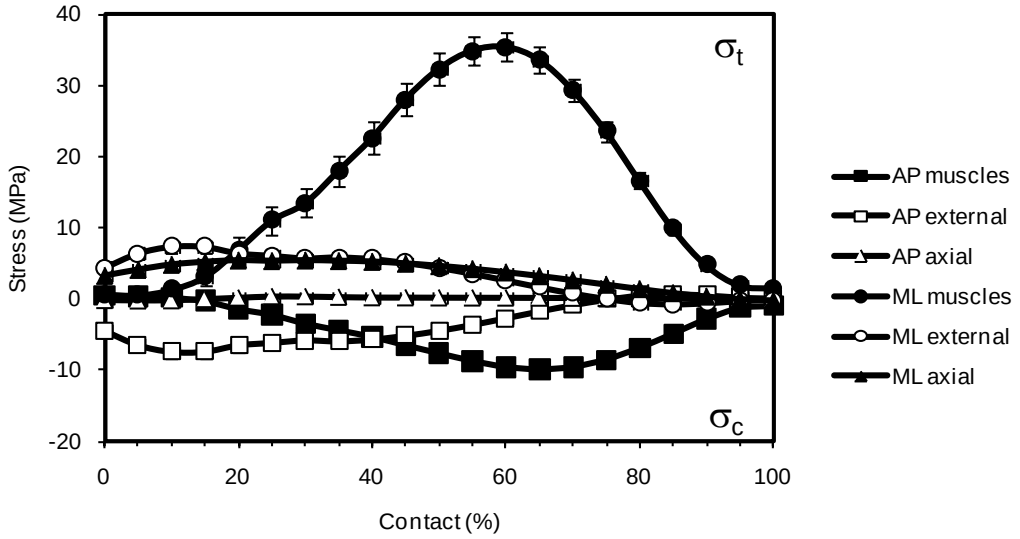

Components of bending stress in the femur induced by muscles and GRF components from the femur of opossums. All plots show means (±s.e.m.) averaged across all four opossums (N=8-20 trials per individual, 56 total steps per data point). Stresses plotted are those occurring on the lateral surface for forces acting to cause mediolateral (ML) bending, and those occurring on the anterior surface for forces acting to cause anteroposterior (AP) bending. Tensile stress is positive and compressive stress is negative. 'Muscles' indicates stresses induced by major muscle groups in the direction indicated; 'external' indicates stresses induced by the GRF acting in the direction indicated; 'axial' indicates stresses induced by the axial component of the GRF due to bone curvature in the direction indicated. Bending stresses induced by axial forces are relatively small and overlap along the zero line for the AP direction.

Figure 7. Loading regime of the right femur at peak tensile stress

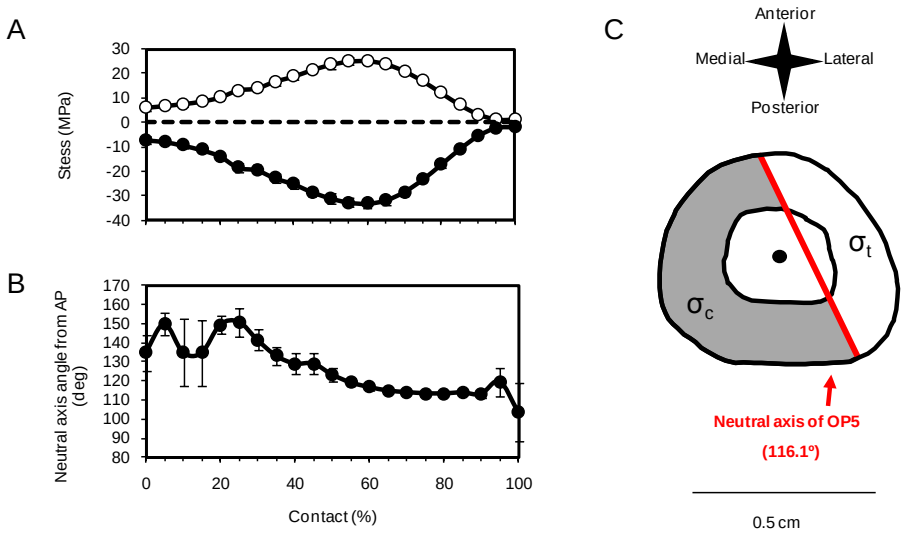

(A) Maximum tensile (σ_t, open circles) and compressive (σ_c, closed circles) stresses acting in the right femur and (B) neutral axis angle from the anatomical ML axis for the femur of opossums. All plots show means (±s.e.m.) averaged across all four opossums (N=8-20 trials per individual, 56 total steps per data point). (C) Schematic cross-section of a right femur illustrating neutral axis orientation for bending (red line and values) at peak tensile stress for one individual (OP5). Neutral axis is illustrated offset from the centroid (dark circle) due to axial compression superimposed on bending loads. The medial cortex of the femur experiences compression (shaded) and the lateral cortex experiences tension (unshaded).